Comparison of Electrical and Microtensile Evaluations of Mechanical Properties of an Aluminum Film

N. BARBOSA, III, R.R. KELLER, D.T. READ, R.H. GEISS, and R.P. VINCI

We compare two types of tests for measurement of mechanical properties of thin films and small scale structures: a microtensile test and a thermomechanical fatigue test induced by alternating current at low frequency and high current density. The microtensile test was used as a reference for evaluating the feasibility of using the electrical test for measurement of mechanical properties. Tests were performed on structures cofabricated from thin film Al deposited on Si to ensure comparable mechanical properties. The films had a grain diameter of 220 nm and a thickness of 1.9 μm. The electrical test resulted in an estimated ultimate tensile strength of 250 $\pm$ 40 MPa. This value was based on extrapolation of high-cycle fatigue data to one reversal through a modified Basquin equation while accounting for varying mean stress. An ultimate tensile strength of 239 $\pm$ 4 MPa was determined from the microtensile test. Differences between these values are explained in terms of the effects of substrate constraint on the strength of the thin film. We conclude that electrical testing methods offer a feasible means for measuring mechanical properties of individual patterned structures.

DOI: 10.1007/s11661-007-9112-y

I. INTRODUCTION

RELIABILITY prediction for thin films used in microelectronic interconnects and microelectromechanical system (MEMS) components has been a challenge for scientists and engineers for the past several decades. A significant amount of research has been aimed at understanding material behavior at small scales, in order to enable better reliability prediction for design purposes. Early work indicated that materials parameters such as yield strength, an important input for the reliable design of components exposed to strains, may not be extrapolated from bulk materials.[1,2] Later work confirmed that as film thickness approached the size scale of the microstructural features of the constituent film, certain mechanical properties such as hardness and strength increased for thinner films, while the elastic properties remained unchanged.[3,4] It is clear that the interaction between length scales associated with the thickness and microstructure of a film and the length scales associated with dislocation plasticity plays a major role in determining the strength of a particular film.[4,5]

N. BARBOSA, III, Materials Research Engineer, R.R. KELLER, Group Leader, D.T. READ, Physicist, and R.H. GEISS, Materials Research Engineer, are with the National Institute of Standards and Technology, Boulder, CO, USA. Contact e-mail: barbosa@boulder.nist.gov R.P. VINCI, Assistant Professor, is with the Department of Materials Science and Engineering, Lehigh University, Bethlehem, PA 18015, USA.

This article is based on a presentation given in the symposium entitled "Deformation and Fracture from Nano to Macro: A Symposium Honoring W.W. Gerberich's 70th Birthday," which occurred during the TMS Annual Meeting, March 12–16, 2006 in San Antonio, Texas and was sponsored by the Mechanical Behavior of Materials and Nanomechanical Behavior Committees of TMS.

Methods used for measuring mechanical properties in bulk materials are typically not suitable for use at micrometer and nanometer length scales due to difficulty in specimen preparation, specimen handling, and the application and measurement of loads and displacements. Uniaxial monotonic testing has long been acknowledged as the primary method for measuring tensile and cyclic properties of bulk materials. However, this approach is particularly difficult at the micrometer and nanometer scales. Initial attempts to perform uniaxial tensile tests on films (*i.e.*, microtensile tests) were performed through careful modification of existing large scale test equipment and methods to grip and test film specimens tens to hundreds of micrometers thick.[6,7,8] As film dimensions decreased, new methods for improved specimen handling and test actuation were required. Specimens were made more robust by fabricating them on silicon substrates. In some cases, the Si supports were removed after specimen gripping,[9,10] and in other cases, the Si remained in place during actuation.[11] Handling and actuation were further improved through increasingly complex methods that progressed from actuation through gripping a single end of the specimen with a micropositioned hook,[12] to mounting self-aligning samples on loading pins.[10,13] In addition, alternate methods for producing uniaxial strains in specimens through out-of-plane deflection were introduced.[14,15] Currently, on-chip actuation requiring no gripping is the state-of-the-art method for testing.[16]

Displacement measurement and force measurement have similarly moved from techniques developed for bulk materials to those designed for the micro- and nanoscales. Strain measurement is now performed through any of a number of methods including *in-situ*

X-ray diffraction,[17] on-chip displacement gages,[13] and interferometry.[15] Force can be measured through standard load cells or through on-chip force sensors.[13] In combination with the improvements in handling and actuation, force measurement and displacement measurement improvements have allowed for samples of sizes down to 100-nm thick by 10-μm long by 2-μm wide to be tested in unique laboratory systems.

One use of macroscale tensile testing is the evaluation of the dynamic performance of materials under fatigue or creep conditions. Fatigue data are often reported for fully reversed, tension-compression fatigue. At the microtensile scale, samples rapidly buckle under diminutive compressive loads making fully reversed fatigue testing difficult. One solution is to attach test films to elastic substrates, whereby tensile loads and compressive loads could be applied to test specimens.[18] While this solution has been highly successful in investigating the role of film thickness on defect structure development, questions still remain regarding differences in behavior between substrate-supported films and free-standing films under cyclic conditions.

Though increasingly complex methods have been implemented to investigate thin films with ever-decreasing dimensions *via* microtensile tests, industry has yet to fully embrace the method. The primary hindrance to full acceptance outside the research laboratory setting is the complex nature of the sample preparation, the test equipment, and the performance of tests. Alternative methods to provide mechanical property data have been developed for use in lieu of or in addition to the microtensile tests. Wafer curvature,[19] beam bending,[20] bulge testing,[21] and nanoindentation[22] are among the most often reported in the literature, and while all have advantages and limitations, none of these tests are as unambiguous as the microtensile test. In addition, most of these test methods are limited to the determination of properties from blanket thin films that are dissimilar to relevant interconnect line structures and MEMS/NEMS structures of interest. Only nanoindentation and microtensile testing have the ability to test individual patterned structures.

The a.c. thermomechanical technique (AC) was first related to mechanical fatigue by Philofsky *et al.*,[23] and later developed further by Keller *et al.*[24] In principle, the test method had many of the desired aspects of wafer curvature testing, beam bend testing, and microtensile testing, while also offering the potential for determining the fatigue properties of individual patterned structures and buried structures through simple electrical contact. Drawbacks include variable temperature induced in the lines during the test and the inability to measure stress. Further, questions remain regarding how the mechanisms active in this test relate to fatigue and thermomechanical fatigue in thin films.

The microtensile testing technique (MT) has been shown to be a primary method for the determination of the elastic and plastic properties of freestanding thin films.[12] A comparison of results determined from this reference technique to the results obtained from the AC demonstrate the ability of the electrical technique to estimate mechanical properties.

One relation that has been shown to correlate fatigue lifetime data and monotonic tensile properties is the Basquin equation:

$$\sigma_a = \sigma_f^{'}(2N_f)^b \qquad [1]$$

which relates the stress amplitude σ_a to the number of reversals to failure N_f through the fatigue strength coefficient $\sigma_f^{'}$ and the fatigue strength exponent b. The relationship between cyclic properties and monotonic properties becomes clear upon realization that the fatigue strength coefficient is to a good approximation equal to the true fracture strength found in a monotonic tension test.[25] When necking is taken into consideration, the Basquin strength coefficient can also be related to the ultimate tensile strength.

In this work, we demonstrate a measurement approach to obtain the ultimate tensile strength by means of an a.c.-driven electrical technique and compare the results with those obtained through a microtensile technique.

II. EXPERIMENTAL PROCEDURE

A. *Specimens*

The AC and MT specimens were fabricated using conventional microelectronics cleanroom techniques. Samples were thermally evaporated from 99.999 pct pure Al wire. The material for all AC and MT samples tested in this work was deposited onto one single-side polished wafer during the same deposition step. The Al was then patterned with subtractive lithography and individual dies were removed from the wafer using a high-speed dicing saw. Following dicing, individual dies were cleaned and the MT samples were subjected to an additional XeF_2 etching step to release the metal structures. Comparable samples, with constant grain size and thickness, were assured through simultaneous processing. Table I summarizes sample dimensions and grain diameters. Thickness was measured with a profilometer. Specimen widths, grain diameter, and crystallographic orientations were measured with a scanning electron microscope (SEM) equipped with electron backscatter diffraction (EBSD). Specimen lengths were determined through light optical microscopy (LOM).

B. *Microtensile Testing*

Microtensile tests were performed with a fixed-end and hook style setup, as previously described elsewhere.[12] Alignment and sample straining were observed through a LOM mounted on an electrical probe station with a stage allowing for sample rotation as well as independent x, y, and z translations. The samples, the fabrication of which is described subsequently, were arranged on a die in an 8×4 array and were nominally 200-μm long, 10-μm wide, and 1.8-μm thick, as shown in Fig. 1. For testing, the sample die was affixed to a stub with silver paste and the stub was mechanically clamped into the specimen stage. Rotational loading

Table I. Sample Geometries and Grain Sizes: the Thickness was Determined through Profilometry, the Widths Were Determined through SEM Imaging, the Lengths Were Determined through LOM Imaging, and the Grain Diameter Was Determined through Automated EBSD Analysis

Specimen type	Thickness (μm)	Width (μm)	Length (μm)	Grain Diameter (nm)
MT—as deposited	1.853 ± 0.006	14.9 ± 0.7	186.7 ± 0.2	220
AC—as deposited	1.853 ± 0.006	5.7 ± 0.3	398.2 ± 0.4	220

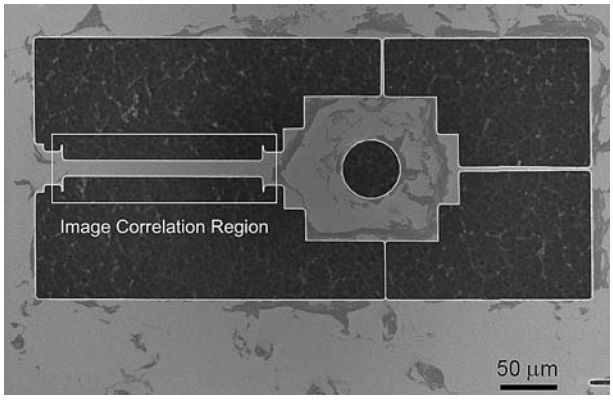

Fig. 1—Individual microtensile sample showing the gage section and image correlation flags on the left side of the image, the round pull hole in the center of the image, and the three tethers on the top, middle, and right sides of the image. Prior to testing, the tethers are removed mechanically. The rough area underneath the sample is the Si wafer, which has been etched to a depth of approximately 100 μm through a gaseous XeF_2 process. The secondary electron image was taken at an accelerating voltage of 15 kV.

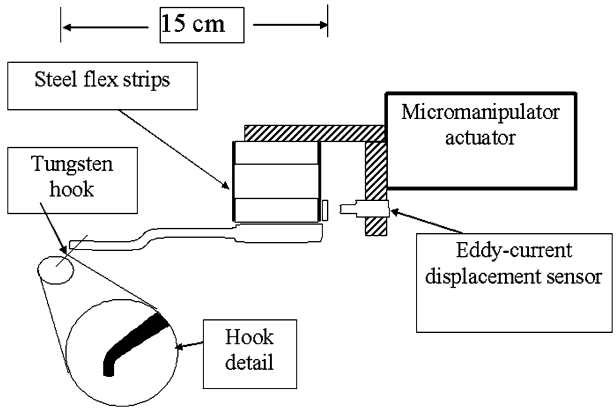

Fig. 2—Schematic depicting the actuation hook and load cell of the microtensile test system.

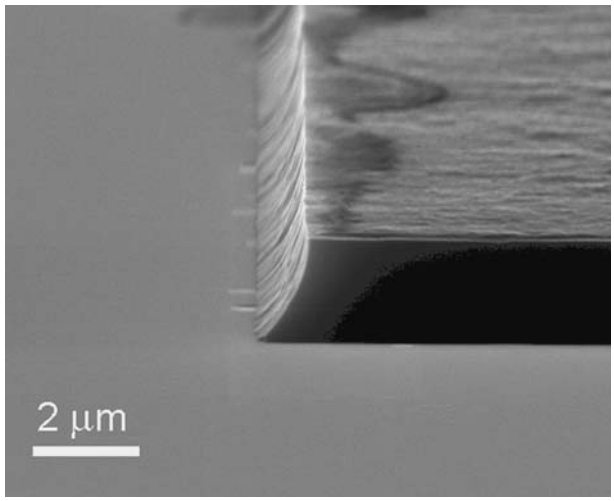

Fig. 3—Typical sidewall profile formed through subtractive patterning during fabrication. The secondary electron image was taken at an accelerating voltage of 15 kV and a tilt of 85 deg.

axis alignment was manually performed and then fixed for a particular die. The tethers, which provide sample stability during the final etch step, were severed prior to testing by means of mechanical shearing *via* the actuation hook. An inchworm piezoelectric three-axis micromanipulator was used to engage the hook in the sample pull hole and apply tension. The tungsten actuation hook was affixed on the load cell, which consists of an eddy-current displacement sensor and two steel flexure strips. The micromanipulator was controlled by custom software, which records displacements and loads and sends a timing signal to the image capture software controlling the camera mounted on the LOM. A schematic of the load cell and pull hook is shown in Fig. 2. Microtensile tests were run to specimen failure after the inclusion of several intermittent unloading steps in order to obtain the elastic modulus from the unloading curve.

Six MT samples were strained to failure at a displacement rate of 13 μm/min. Strain was determined through digital image correlation,[12,26] which used images captured at 3-second intervals during testing. Figure 1 shows the region imaged during testing as well as marker flags located at each end of the gage section. The marker flags were used for displacement measurements during the post-test analysis. A 250-nm pixel size combined with a relative displacement resolution of 0.02 pixels defined the minimum strain resolution to be 5 nm or 25 microstrain on a sample with a 200-μm gage length.

Stress was calculated from the instantaneous load and initial cross-sectional area. A stress resolution of 30 MPa was determined by combining the 30 μN force resolution[12] with the 1 μm^2 uncertainty in cross-sectional area. Film thickness was measured with a mechanical profilometer capable of 5-nm resolution. Sample width was measured with a scanning electron microscope calibrated to be within 5 pct of the true magnification value. Fig. 3 shows the sidewall profile of a specimen to be curved, an artifact of the subtractive patterning process. The full-width at half-maximum sample height was used to account for the curved specimen sidewalls in the calculation of cross-sectional areas.

C. *AC Testing*

The AC tests were performed in a system capable of application of a sinusoidal current of a predetermined current density through a line while at the same time monitoring changes in line resistance. The sinusoidal current density was applied at a frequency of 100 Hz, causing 200 Hz power cycles and therefore 200 Hz temperature cycles. Lifetime data were generated by contacting a sample with the four-point probe system and then applying a current until the resistance of the sample indicated open circuit. The use of a 100 Hz frequency allows for a high number of cycles in a short amount of time, but does not approach the maximum effective test frequency, which is limited by the efficiency of heat transfer out of the interconnect.[27] Strains in the sample are determined by the mismatch in the coefficient of thermal expansion (CTE) experienced between the metal line ($\alpha_{Al} = 23.1 \times 10^{-6}$ °C^{-1}) and the silicon substrate ($\alpha_{Si} = 2.6 \times 10^{-6}$ °C^{-1}). Control of the imposed strains was accomplished by varying the current density. The cyclic strain range ($\Delta\varepsilon$) due to thermal expansion mismatch ($\Delta\alpha$) is defined as

$$\Delta\varepsilon = \Delta\alpha\Delta T \quad [2]$$

where ΔT is the cyclic temperature excursion. The temperature in our test lines was determined by use of four-point resistivity measurements through the relation

$$R(T) = R_0 + \Delta T\left(\frac{d\rho}{dT}\right)\left(\frac{L}{A}\right) \quad [3]$$

where R_0 is the initial resistance measured at a known temperature, $d\rho/dT$ is the change in resistivity with temperature, L is the line length, and A is the cross-sectional area of the line. Equation [3] assumes Matthiessen's rule applies. A $d\rho/dT$ of 0.01134 $\mu\Omega$ cm/°C for Al was used in this work.[28] The fatigue life curve was determined by applying a number of different current amplitudes while monitoring resistance to determine the number of cycles to open circuit. The uncertainty in the ability to measure the root mean square (RMS) resistance value was determined to be ± 0.04 Ω RMS.

Tests were performed with the chuck temperature of the probe station held at a constant 20 °C. Chuck temperature uncertainty is estimated to be 0.5 °C. The RMS current densities were between 11.65 and 12.3 MA/cm^2. Uncertainty in the measurement of RMS current was determined to be ± 0.05 mA. Resistance measurements were made through a four-point contact method where a known current was passed through a line and the voltage was monitored. Stress amplitudes were determined from strain amplitudes, based on measured line temperatures and moduli of elasticity.

III. RESULTS

Figure 4 shows the stress-strain curves constructed with the data acquired from the microtensile tests. Uncertainties in the modulus of elasticity, 0.2 pct offset yield stress, and ultimate tensile strength measured by monotonic uniaxial tests were all less than 10 pct of the measured values. The relative uncertainty in the measurement of the average elongation at failure was slightly higher at 13 pct. Though the strain uncertainty at any data point remains constant throughout a test, an increase in the strain interval between data points at higher strains can be seen in Fig. 4. The variation in the strain interval is due to the nonrigid (compliant) load train used. Early in the test, displacement imposed at the actuator is accommodated by several load train members outside of the gage section as well as by the gage section. As testing proceeds, the gage section yields but the rest of the load train does not, so larger percentages of the total imposed displacement are accommodated by the gage section resulting in larger strain intervals per unit time.

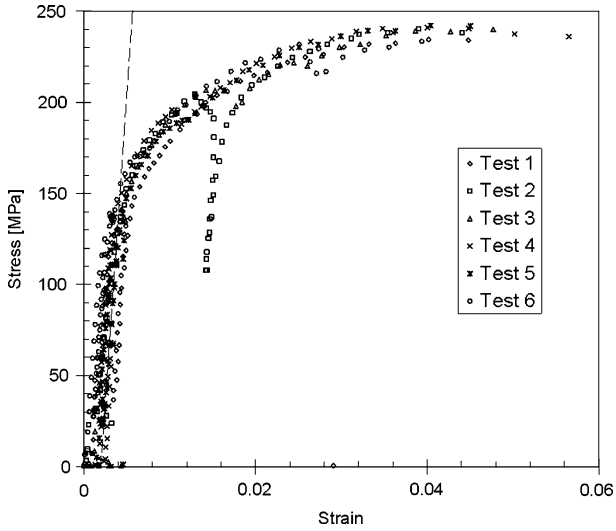

Fig. 4—Stress-strain data for six microtensile tests showing the reproducibility of the test. The dashed line shows the calculated modulus at a 0.2 pct strain offset.

Failure in all cases occurred at less than 6 pct elongation with an average elongation at failure equal to 4.6 ± 0.6 pct. The modulus of elasticity as calculated from the unloading curves was determined to be 68 ± 6 GPa. An example of an intermediate unloading curve from which the elastic modulus was calculated may be seen in the test 2 data shown in Fig. 4 at a strain of approximately 1.25 pct. Intermediate unloading data for the other tests is difficult to distinguish in Fig. 4 as they occur at less than 1 pct strain. The 0.2 pct offset yield stress was calculated to be 140 ± 10 MPa, and the ultimate tensile strength was calculated at 239 ± 4 MPa.

A typical fracture of the MT samples can be seen in Fig. 5. The fracture occurred obliquely, traversing the sample. From the image, there appears to be a significant amount of localized plasticity within 1 to 2 μm of the fracture edge and limited necking prior to failure.

Residual stress due to deposition without substrate cooling was estimated to be 240 MPa, consistent with literature values measured for Al films.[29,30] An S-N curve determined through the AC method is shown in Fig. 6. A Basquin power-law fit yielded a fatigue strength coefficient of 350 ± 60 MPa and a fatigue

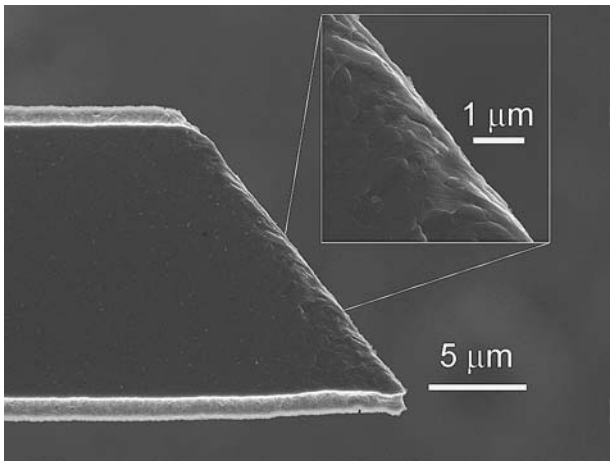

Fig. 5—A typical microtensile sample fracture. Localized necking appears to be confined to a 1- to 2-μm region local to the fracture surface. In samples where limited necking occurs, the true fracture strength and the ultimate tensile strength are approximately equal. The secondary electron image was taken at an accelerating voltage of 5 kV. The viewing direction is normal to the film surface.

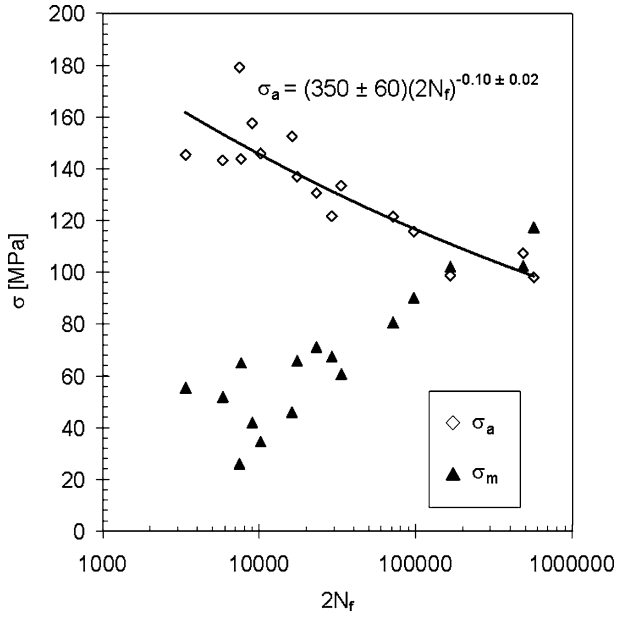

Fig. 6—An S-N plot for electrical AC tests showing the stress amplitude σ_a and mean stress σ_m as functions of cycles. The equation relating stress amplitude to cycle number was determined by performing a power-law nonlinear regression. The power-law equation was of the form used by the Basquin equation to describe fully reversed cyclic deformation in the elastic stress amplitude range. Due to an experimental idiosyncrasy, the mean stress in this experiment increases with decreasing stress amplitudes.

exponent of -0.10 ± 0.02. The mean stress (σ_m) is defined as

$$\sigma_m = \frac{\sigma_{\max} + \sigma_{\min}}{2} \quad [4]$$

where $\sigma_{\max}$ is the maximum stress and $\sigma_{\min}$ is the minimum stress in one cycle, measured in the AC tests. The term σ_m is shown in Fig. 6 to increase with decreasing stress amplitude. The inverse relationship between the mean stress and stress amplitude is a consequence of the experimental technique. Namely, from an initial state of residual tension, heating reduces the stress, so less heating (lower current density) implies higher mean stress.

IV. DISCUSSION

The modulus of bulk Al is reported to be 70.6 GPa,[31] which falls within the 95 pct confidence interval determined for the measured value of 68 ± 6 GPa. This result is not surprising because the modulus of a material is dependent on the atomic bond properties, which have not been shown to change at the length scale of interest. Previously, the modulus of elasticity has proven difficult to accurately measure with measured values often as much as 20 pct lower than the literature value for the modulus of elasticity.[32,33] The accurate measurement of the bulk modulus of elasticity assures confidence in sample preparation and measurement of further monotonic properties.

Using fatigue testing to determine monotonic properties such as ultimate tensile strength is a nonconventional approach. If a comparison between cyclic and monotonic properties is made, it is typically monotonic properties that are used to estimate cyclic properties. However, we are attempting the opposite. Extensive work has been reported regarding the estimation of fatigue life data from monotonic tests[34] as well as from limited fatigue data.[35] A starting point for analysis of cyclic deformation with elastic strain amplitudes is the use of a power-law fit as applied to the AC data in Fig. 6. This fit is typical of the Basquin relation [1], which was developed to characterize the lifetime properties of fully reversed cyclic loading in the elastic regime. The goal of this work is to relate the ultimate tensile strength determined from a MT test to the fatigue strength coefficient determined through AC tests. The fatigue strength coefficient has been correlated to the true fracture stress,[36] which is defined as the load at fracture divided by the instantaneous cross-sectional area. A plot showing data relating the fatigue strength coefficient to the true fracture strength in 47 materials may be found in Fig. 7.

In the case of the MT samples, very little necking was observed in the test specimen (Fig. 5). Further, a distinct maximum followed by reduction in engineering stress was not indicated in the stress-strain curves (Fig. 4). This allows for the substitution of the ultimate tensile strength as the true fracture stress in the original Basquin relation (Eq. [1]). With these assumptions, the electrically measured fatigue strength coefficient of 350 ± 60 MPa gives a first estimate of the ultimate strength. It is clear that this value grossly exceeds the value of 239 ± 4 MPa as determined by microtensile testing. Thin-film yield strengths have been shown to be over 100 MPa larger than those found in their bulk counterparts due to some combination of substrate constraint and the small grain sizes in the films;[5,37]

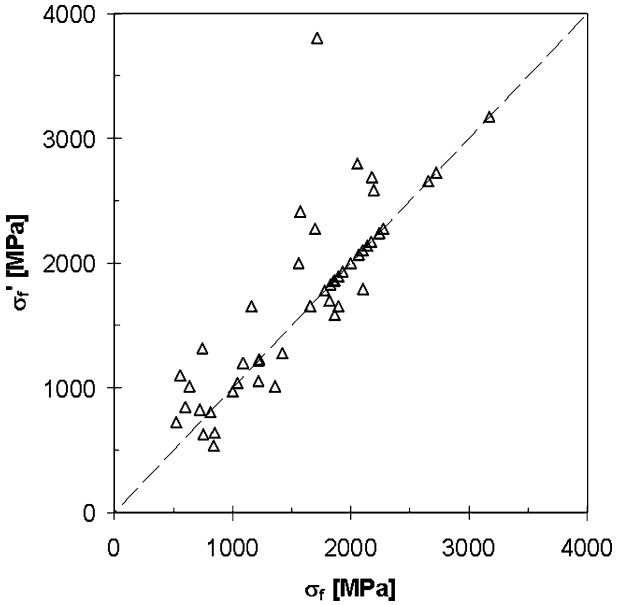

Fig. 7—The fatigue strength coefficient σ_f' plotted *vs* the true fracture strength σ_f of selected steels, aluminum alloys, and titanium alloys.[40] The fatigue strength coefficients were determined through the Basquin equation used to fit fully reversed fatigue, and the true fracture strengths were determined through monotonic tensile tests. The dashed line represents the case where the fatigue strength coefficient is equal to the true fracture strength. The high percentage of data points in close proximity to the line demonstrates the correlation between the two values.

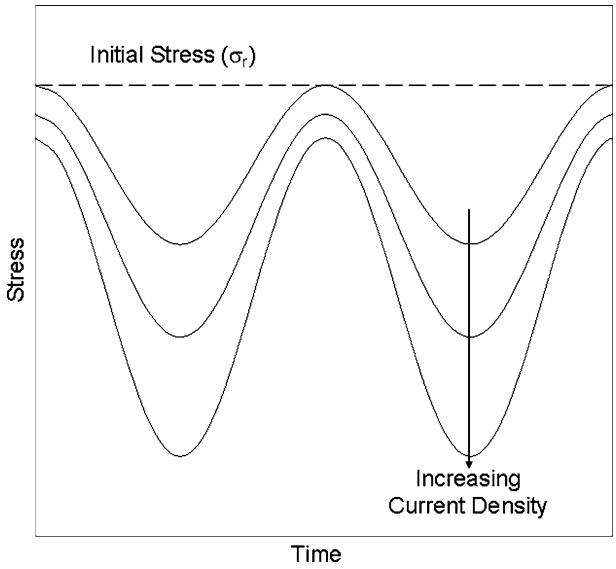

Fig. 8—A schematic showing the effect of increasing current density on the resulting steady-state stress cycling during testing. The maximum test stress is the initial stress denoted by the dashed horizontal line. The initial stress may only be increased by lowering the initial chip temperature, assuming that the film stress is not at the maximum sustainable stress. At small current densities, the stress in the sample is driven in the compressive direction by the increasing line temperature, finally reaching a minimum value of stress before returning to the initial stress. As the current density increases, not only is the stress amplitude increased, but the peak stress no longer returns to the initial stress due to heat dissipation from the line into the chip. Both of these processes effectively reduce the mean stress.

however, in this case, the grain size is the same in the MT and AC samples leaving the substrate constraint alone to account for differences in strength levels.

The effect of substrate constraint alone is insufficient, however, for accounting for the total discrepancy between the electrical result and the mechanical result. Electrical tests of fatigue, as conducted here, contain a significant nonzero mean stress, which must be considered during use of the Basquin relation. It is known that tensile mean stresses during cyclic deformation reduce lifetime in most materials from the lifetime determined by fully reversed tests.[36,38] Several methods have been developed to account for this. In one approach, Morrow[39] suggests incorporation of the mean stress into the original Basquin equation:

$$\sigma_a = \left(\sigma_f^{'} - \sigma_m\right)\left(2N_f\right)^b \qquad [5]$$

From Eq. [1], the intercept of a log-log plot of the stress amplitude *vs* cycles to failure is equal to the fatigue strength coefficient. The intercept of such a plot constructed from Eq. [5] is a combination of the mean stress and the fatigue strength coefficient. If a mean stress from the data in Fig. 6 can be estimated, it may then be used to determine a fatigue strength coefficient that is closer to the ultimate tensile strength determined in the MT tests.

Due to the nature of the experimental setup, not only is a mean stress present, but it is a nonconstant mean stress, increasing with decreasing stress amplitude. In order to better understand the generation of the varying mean stress, it is useful to re-examine the nature of the AC test. As previously mentioned, the maximum tensile stress sustained by the film is equal to the residual thermal stress σ_r developed during and after processing. In Figure 8, this stress is denoted by the dashed line. As a sinusoidal current with a constant RMS value is passed through the sample, the stress cycles between two fixed values. Fig. 8 is a schematic depicting three different RMS sinusoidal currents after having reached steady state. The smallest current density produces cycles that alternate between the initial stress and some smaller stress value. This case has the smallest stress amplitude but the largest mean stress. By increasing the amplitude of the stress cycling, through an increase in the RMS current density, the peak stress no longer reaches the initial stress value. This change in peak stress is due to increases in the steady-state chip temperature due to the dissipation of the joule heat of the line. This increase in chip temperature is the cause for the shift in mean stress shown in Fig. 6.

Schematically, Fig. 9 shows the effect of increasing mean stress (decreasing current density) on fatigue lifetime curves. The figure shows a series of hypothetical fatigue life curves (dashed lines) for cyclic loading in the elastic range. The S-N curves shift to lower stress amplitudes as mean stress increases (current density decreases). The topmost schematic curve is the case of fully reversed loading (mean stress equal to zero),

possibly under conditions of very high current density and substrate cooling. As the mean stress increases, the stress intercepts are shifted downward. The variable mean stress curve, indicated by the solid dark line, shows an effect that changing chip temperature necessarily introduces during cycling at different current densities. As the mean stress is reduced at higher current densities throughout the course of determining one S-N curve, the fatigue strength coefficient and exponent dynamically change, requiring a modified approach to extrapolating the final strength coefficient at one load reversal.

Fig. 9 depicts a key fundamental difference between mechanical tests and the electrically induced fatigue tests described in this work. In the electrically induced test, the mean stress and stress amplitude are necessarily inversely coupled, because there was no active control of substrate temperature. This coupling is not present in mechanical fatigue testing. It can be eliminated in an electrical test through substrate cooling controlled by a feedback loop designed to maintain either a constant mean or maximum temperature.

A nonlinear regression technique was used to determine the fatigue strength coefficient and exponent from Eq. [5] in combination with the fatigue amplitude and cycles to failure data while accounting for the varying mean stress. A fatigue strength coefficient of 250 ± 40 MPa and a fatigue strength exponent of −0.03 ± 0.02 were determined through this method. In Fig. 10, the solid line shows the modified Basquin equation for the case of zero mean stress using the parameters determined through the regression. The dashed lines show the cases of the modified Basquin equation with constant mean stresses of 42, 71, and 102 MPa. In each case, proximity of the dashed curves

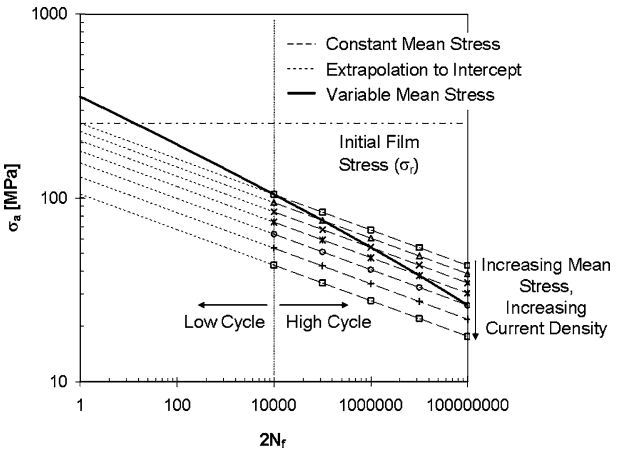

Fig. 9—An S-N schematic of the effect of decreasing mean stress with increasing current density, where σ_a is the stress amplitude and $2N_f$ is the number of cycles to failure. The parallel dashed lines show the influence of increasing mean stress on fatigue life curves with constant mean stress derived from Eq. [5]. The topmost dashed line is the case of fully reversed fatigue. The solid line is representative of the test data, which have a mean stress that increases with decreasing stress amplitude. Data are limited to the region beyond 10^4 cycles because this is typically considered to be the region where Basquin-type equations are valid; the short dashes show the effect of mean stress on the intercept of the curves.

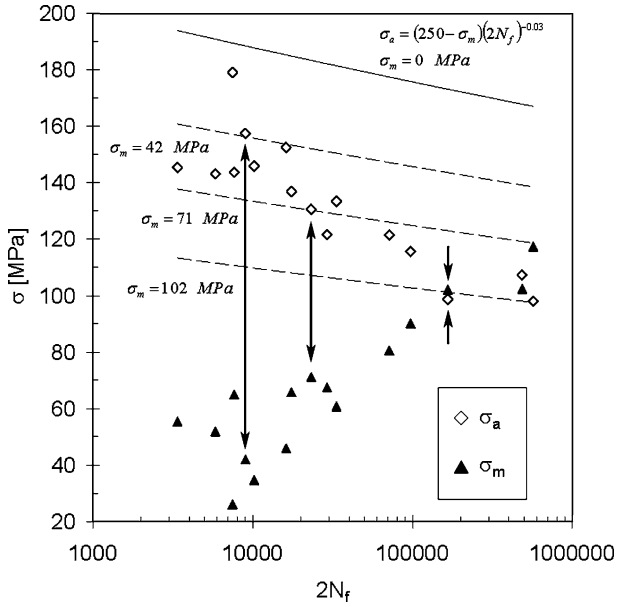

Fig. 10—Results of the data analysis on an S-N plot for electrical AC tests showing the stress amplitude σ_a and mean stress σ_m as functions of cycles to failure $2N_f$. The solid line is the result of the nonlinear regression of stress amplitude as a function of mean stress and cycles to failure and represents the curve for fully reversed fatigue. The dashed lines represent curves determined for the mean stress values 42, 71, and 102 MPa. The lines graphically show the ability of the analysis technique to capture the dependence of stress amplitude on mean stress and cycles to failure through their proximity to data points with mean stresses of the same level.

to the stress amplitude data point determined under the same mean stress conditions displays the ability of the model to capture the dependence of lifetime on fatigue amplitude and mean stress. A comparison of Fig. 10 to Fig. 9 will show that the analysis produced results consistent with the experiment description.

The experimentally determined best estimate fatigue strength coefficient (ultimate tensile strength) of 250 ± 40 MPa found through the modified analysis falls within the 95 pct confidence interval, 239 ± 4 MPa, determined for the MT ultimate tensile strength value. The electrically determined value is slightly higher, but any differences may be accounted for by substrate constraint strengthening. In contrast, the best estimate fatigue strength exponent lies outside the range of −0.05 to −0.12 typical of most metals. The lowest value of the 95 pct confidence interval overlaps the "rule-of-thumb" range, but the 67 pct uncertainty is cause for some concern. As the mechanisms underlying the deformation are not yet fully understood, further experiments are required to understand the source of uncertainty.

V. CONCLUSIONS

Through an electrically driven thermal cycling approach, and a data analysis procedure that considers the effect of mean stress on fatigue lifetime, we have estimated the ultimate tensile strength of an Al thin film

to be 250 ± 40 MPa, which compares to a value of 239 ± 4 MPa as determined through microtensile testing. This is the first report of an ultimate tensile strength derived from an electrically driven fatigue test for thin films. The effects of residual tensile stress in the specimen films, the effective temperature of the specimen, and the strengthening due to substrate constraint require further exploration. The small 5 pct error between strength results determined from the two test types indicates that the electrically driven test may be a useful means of obtaining strength values normally measured in monotonic tests.

ACKNOWLEDGMENTS

We thank the NIST Office of Microelectronics Programs for support. This research was performed while one of the authors (NB) held a National Research Council Research Associateship Award at NIST. We gratefully acknowledge support from the National Science Foundation, Grant Nos. DMR-9876261 and ECS-0322702. This work is a contribution of the United States Department of Commerce and is not subject to copyright in the United States.

REFERENCES

1. J.W. Menter and D.W. Pashley: *Structure and Properties of Thin Films*, Wiley, New York, NY, 1959, pp. 111–50.
2. R.W. Hoffman: *Physics of Thin Films*, Academic, New York, NY, 1966, pp. 211–73.
3. F.R. Brotzen: *Int. Mater. Rev.*, 1994, vol. 39, pp. 24–45.
4. E. Arzt: *Acta Mater.*, 1998, vol. 46, pp. 5611–26.
5. W.D. Nix: *Metall. Trans. A*, 1989, vol. 20A, pp. 2217–45.
6. D.M. Marsh: *J. Sci. Instrum.*, 1959, vol. 36, pp. 165–69.
7. C.A. Neugebauer: *J. Appl. Phys.*, 1960, vol. 31, pp. 1096–1101.
8. M. Spivack: *Rev. Sci. Instrum.*, 1972, vol. 43, pp. 985–90.
9. D. Read and J. Dally: *Advances in Electronic Packaging 1993*, Proc. 1993 ASME Int. Electronics Packaging Conf., ASME, New York, NY, 1993, pp. 163–69.
10. R.D. Emery and G.L. Povirk: *Acta Mater.*, 2003, vol. 51, pp. 2067–78.
11. L. Fan, R. Howe, and R. Muller: *Sens. Actuators, A (Phys.)*, 1990, vol. A23, pp. 872–74.
12. Y.W. Cheng, D.T. Read, J.D. McColskey, and J.E. Wright: *Thin Solid Films*, 2005, vol. 484, pp. 426–32.
13. M. Haque and M. Saif: *Sens. Actuators, A*, 2002, vols. A97–A98, pp. 239–45.
14. M. de Boer, B. Jensen, and F. Bitsie: *Proc. SPIE–Int. Soc. Opt. Eng.*, 1999, vol. 3875, pp. 97–103.
15. H. Espinosa, B. Prorok, and M. Fischer: *J. Mech. Phys. Solids*, 2003, vol. 51, pp. 47–67.
16. M. Haque and M. Saif: *J. Microelectromech. Syst.*, 2001, vol. 10, pp. 146–52.
17. M. Hommel, O. Kraft, and E. Arzt: *J. Mater. Res.*, 1999, vol. 14, pp. 2373–76.
18. R. Schwaiger, G. Dehm, and O. Kraft: *Phil. Mag.*, 2003, vol. 83, pp. 693–710.
19. M. Doerner, D. Gardner, and W. Nix: *J. Mater. Res.*, 1986, vol. 1, pp. 845–51.
20. R. Schwaiger and O. Kraft: *Acta Mater.*, 2003, vol. 51, pp. 195–206.
21. Yong Xiang, Xi Chen, and Joost J. Vlassak: *Mater. Res. Soc. Symp. Proc.*, 2002, vol. 695, pp. 189–94.
22. M. Doerner and W. Nix: *J. Mater. Res.*, 1986, vol. 1, pp. 601–09.
23. E. Philofsky, K. Ravi, E. Hall, and J. Black: *9th Ann. Proc. Reliability Physics*, IEEE, New York, NY, 1971, pp. 120–28.
24. R.R. Keller, R. Monig, C.A. Volkert, E. Arzt, R. Schwaiger, and O. Kraft: *AIP Conf. Proc.*, AIP, Melville, NY, 2002, vol. 612, pp. 119–32.
25. S. Suresh: *Fatigue of Materials*, 2nd ed., University Press, Cambridge, United Kingdom, 1998, p. 223.
26. M. Sutton, J. Turner, H. Bruck, and T. Chae: *Exper. Mech.*, 1991, vol. 31, pp. 168–77.
27. R. Monig, R.R. Keller, and C.A. Volkert: *Rev. Sci. Instrum.*, 2004, vol. 75, pp. 4997–5004.
28. P.D. Desai, H.M. James, and C.Y. Ho: *J. Phys. Chem. Ref. Data*, 1984, vol. 13, pp. 1131–72.
29. C.A. Volkert, C.F. Alofs, and J.R. Liefting: *J. Mater. Res.*, 1994, vol. 9, pp. 1147–55.
30. R. Venkatraman and J.C. Bravman: *J. Mater. Res.*, 1992, vol. 7, pp. 2040–48.
31. E.A. Brandes and G.B. Brook: *Smithells Metals Handbook*, 7th ed., Butterworth-Heinemann, Oxford, United Kingdom, 1998, chapter 15, p. 2.
32. D.T. Read, Y.W. Cheng, R.R. Keller, and J.D. McColskey: *Scripta Mater.*, 2001, vol. 45, pp. 583–89.
33. R.W. Hoffman: *Mater. Res. Soc. Symp. Proc.*, 1989, vol. 130, pp. 295–306.
34. S.S. Manson: *Exp. Mech.*, 1965, vol. 5, pp. 193–226.
35. S.S. Manson: *Methods for Predicting Material Life in Fatigue*, ASME, New York, NY, 1979, pp. 145–82.
36. S.S. Manson and G.R. Halford: *Fatigue and Durability of Structural Materials*, ASM INTERNATIONAL, Materials Park, OH, 2006, pp. 1–456.
37. W.D. Nix and B. Ilschner: *Energy Technol. Rev.*, 1980, pp. 1503–30.
38. S. Suresh: *Fatigue of Materials*, 2nd ed., University Press, Cambridge, United Kingdom, 1998, pp. 224–27.
39. J.D. Morrow: *Fatigue Design Handbook—Advances in Engineering*, Society of Automotive Engineers, Warrendale, PA, 1968, pp. 21–29.
40. R.W. Landgraf, M.R. Mitchell, and N.R. LaPointe: *Monotonic and Cyclic Properties of Engineering Materials*, Ford Motor Co. Scientific Research Staff, Dearborn, MI, 1972, pp. 1–138.